Title
A Label-Free Platform for Identification of Exosomes from Different Sources.

Journal
ACS sensors, 4(2)

ISSN
2379-3694

Authors
Yan, Zhongbo
Dutta, Suman
Liu, Zirui
et al.

Publication Date
2019-02-01

DOI
10.1021/acssensors.8b01564

Peer reviewed

ACS SENSORS

Article

Cite This: ACS Sens. XXXX, XXX, XXX−XXX

pubs.acs.org/acssensors

A Label-Free Platform for Identification of Exosomes from Different Sources

Zhongbo Yan,[†,#] Suman Dutta,[‡,#] Zirui Liu,[†] Xinke Yu,[†] Neda Mesgarzadeh,[†] Feng Ji,[†] Gal Bitan,[*,‡,§,∥] and Ya-Hong Xie[*,†,⊥]

[†]Department of Materials Science and Engineering, [‡]Department of Neurology, David Geffen School of Medicine, [§]Brain Research Institute, and [∥]Molecular Biology Institute, University of California Los Angeles, Los Angeles, California 90095, United States

[⊥]Jonsson Comprehensive Cancer Center, University of California Los Angeles, Los Angeles, California 90024, United States

Supporting Information

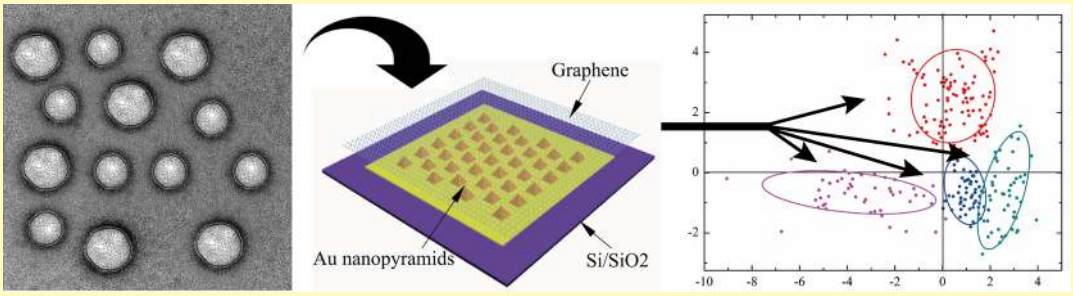

ABSTRACT: Exosomes contain cell- and cell-state-specific cargos of proteins, lipids, and nucleic acids and play significant roles in cell signaling and cell−cell communication. Current research into exosome-based biomarkers has relied largely on analyzing candidate biomarkers, i.e., specific proteins or nucleic acids. However, this approach may miss important biomarkers that are yet to be identified. Alternative approaches are to analyze the entire exosome system, either by "omics" methods or by techniques that provide "fingerprints" of the system without identifying each individual biomolecule component. Here, we describe a platform of the latter type, which is based on surface-enhanced Raman spectroscopy (SERS) in combination with multivariate analysis, and demonstrate the utility of this platform for analyzing exosomes derived from different biological sources. First, we examined whether this analysis could use exosomes isolated from fetal bovine serum using a simple, commercially available isolation kit or necessitates the higher purity achieved by the "gold standard" ultracentrifugation/filtration procedure. Our data demonstrate that the latter method is required for this type of analysis. Having established this requirement, we rigorously analyzed the Raman spectral signature of individual exosomes using a unique, hybrid SERS substrate made of a graphene-covered Au surface containing a quasi-periodic array of pyramids. To examine the source of the Raman signal, we used Raman mapping of low and high spatial resolution combined with morphological identification of exosomes by scanning electron microscopy. Both approaches suggested that the spectra were collected from single exosomes. Finally, we demonstrate for the first time that our platform can distinguish among exosomes from different biological sources based on their Raman signature, a promising approach for developing exosome-based fingerprinting. Our study serves as a solid technological foundation for future exploration of the roles of exosomes in various biological processes and their use as biomarkers for disease diagnosis and treatment monitoring.

KEYWORDS: *exosome, surface-enhanced Raman spectroscopy, graphene, principal component analysis, biomarker*

Extracellular vesicles (EVs) are complex structures comprising a lipid bilayer that contains transmembrane proteins and encloses soluble hydrophilic components derived from the cytosol or other organelles of the donor cell.[1] Exosomes are the most abundant and best-characterized type of EVs, ranging from 30 to 200 nm in diameter. They are produced via the endosomal pathway and are released into the extracellular space from multivesicular bodies.[2] Exosomes play an important role in intercellular communication by transferring biochemical messages among cells.[3] They contain abundant proteins, lipids, and nucleic acids, including mRNA and miRNA, and mediate a wide variety of biological functions.[4] Exosomes have attracted attention for their role in spreading of diseases throughout the affected tissue[5−9] and as a valuable source of biomarkers for diagnosing various diseases, including cancer and neurodegenerative diseases. However, exosome research is still a young field. The scope of biological functions mediated by exosomes and the mechanisms by which they are released from the cells of origin and taken up by recipient cells are yet to be fully elucidated.[10−13]

Received: December 9, 2018
Accepted: January 15, 2019
Published: January 15, 2019

DOI: 10.1021/acssensors.8b01564
ACS Sens. XXXX, XXX, XXX−XXX

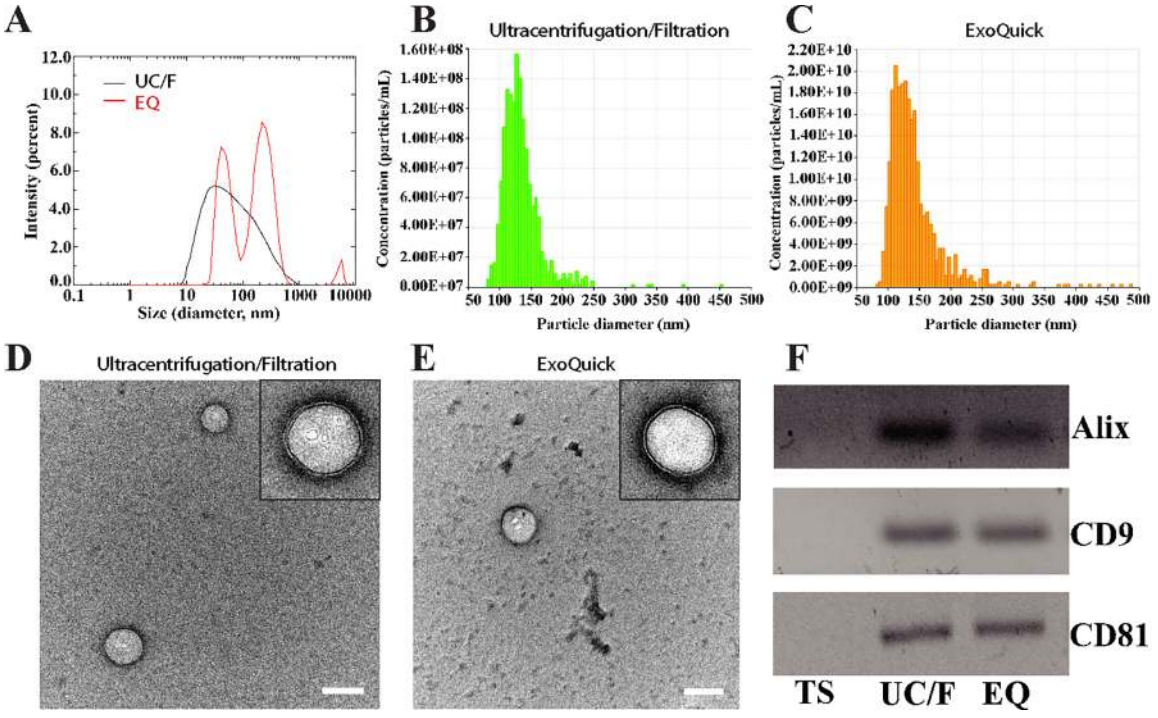

Figure 1. Comparison of exosomes isolated by the ultracentrifugation/filtration method versus the ExoQuick kit. (A) DLS spectra showing the particle size distribution of exosomes isolated by UC/F, (black) or by ExoQuick (EQ, red). (B) TRPS analysis of exosomes isolated by the UC/F method. (C) TRPS analysis of exosomes isolated by the ExoQuick kit. (D, E) Representative TEM image of exosomes isolated by UC/F (D) or ExoQuick (E) at 80,000× magnification. The scale bars in both panels represent 200 nm. The insets show zoomed-in images of a single exosome in each preparation, in which the lipid bilayer is clearly visible. (F) Western blot detecting the exosomal markers Alix, CD9, and CD81. TS: total serum.

Raman spectroscopy is a widely used, label-free, nondestructive method. It has been used for extracting spectroscopic information originating from chemical bonding in molecules, which can in turn be used as fingerprints by which molecules are identified.[14] The label-free nature of Raman spectroscopy has made it a powerful option for studies of biological samples.[15] The most noticeable drawback of Raman spectroscopy, however, is the low yield of Raman scattering events leading to low detection sensitivity.[16] Thankfully, this shortcoming can be overcome by placing the analytes within a few tens of nanometers of nanostructured metallic surfaces,[17−20] a method known as surface-enhanced Raman spectroscopy (SERS) which has been employed extensively and has been demonstrated to have single-molecule sensitivity.[33] One of the unique characteristics of SERS is its very high spatial resolution. When applied to exosomes, the typical lateral spatial separation of SERS hotspots—tens of nanometers apart—makes it inherently a single-exosome analysis even though the typical laser spot size is ∼1 μm. The quadratic dependence of SERS signal intensity on the local electromagnetic field intensity allows the signal from a single plasmonic hotspot to dominate the spectrum collected.[21]

We used a unique plasmonic hybrid platform consisting of a single-layer graphene overlaid on a carefully engineered periodic Au-pyramid nanostructure. The metallic nanostructured surface provides an intense surface plasmonic field upon laser illumination and thus enhances the Raman signal by many orders of magnitude. The graphene layer serves a dual purpose, providing a biocompatible and chemically stable surface, and serving as a built-in gauge of local electromagnetic field intensity enabling quantitative Raman analysis.[22] Previously, the Xie group demonstrated the biocompatibility of the graphene layer successfully by culturing epithelial cells from colon or colon cancer over graphene.[23] Reports by several other groups have also supported the biocompatibility of graphene.[24−27] A critical component of our platform is data analysis used to discern and categorize spectral signatures. Programs suitable for such analysis belong generally in the realm of artificial intelligence. Here, we used a multivariate analysis algorithm known as principal component analysis (PCA).

Our proof-of-concept study presented here contains three parts: (1) characterization of exosomes prepared by two distinct methods and determination of the most suitable one for SERS analysis; (2) establishing the methodology for measuring the Raman signature from single exosomes; and (3) using unbiased PCA to demonstrate unequivocally the separation of exosomes from different biological sources.

RESULTS AND DISCUSSION

Comparison of Exosome Isolation Methods. Two main approaches are used to isolate exosomes. Because they are enclosed by hydrophobic membranes, exosomes (and other EVs) can be precipitated out of solution using simple salting-out reagents, often in the presence of water-soluble polymers, generating relatively heterogeneous mixtures of exosomes, ectosomes, and some protein aggregates and cell debris. Alternatively, a series of differential centrifugation, ultrafiltration, and ultracentrifugation steps[10] (heretofore referred to as ultracentrifugation/filtration (UC/F) method) yields relatively pure exosomes and is considered the "gold standard"

DOI: 10.1021/acssensors.8b01564
ACS Sens. XXXX, XXX, XXX−XXX

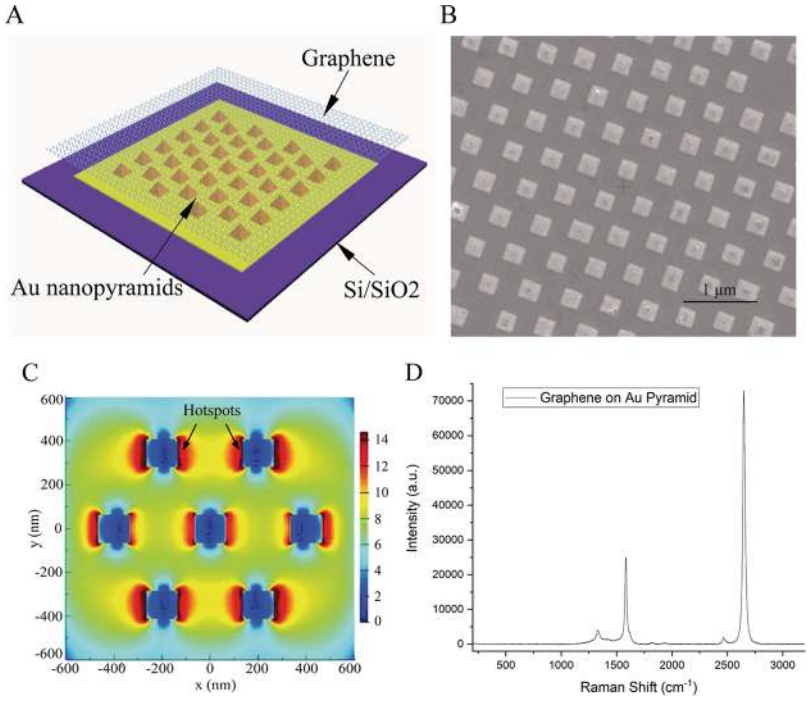

Figure 2. SERS hybrid platform. (A) Schematic diagram of the hybrid platform used in this study. (B) Top-view SEM image of the hybrid platform. (C) Electromagnetic field distribution simulated by FDTD at an input wavelength of 785 nm. The color bar represents the intensity of the electric field. (D) Representative Raman spectrum of the hybrid platform showing the graphene peaks.

in the field. Each method has distinct advantages and disadvantages. The salting-out procedure, often done using commercial kits, such as ExoQuick (Systems Biosciences),[28] is fast and yields nearly 3 orders of magnitude more material,[29] but the resultant EV population is more heterogeneous. In contrast, the UC/F procedure excludes much of the nonexosome components, but it is time-consuming and labor-intensive, achieves low yields, thus requiring larger volume of the initial sample, and can only be used if subsequent analyses are done using high-sensitivity methods. We reasoned that because SERS is a high-sensitivity method, the latter procedure could be used, yet decided to compare the two methods because if using the ExoQuick kit could yield high-quality data, it would require lower sample volumes and allow processing more samples faster.

To compare the two methods, we used fetal bovine serum (FBS). Following isolation of exosomes by each method, we compared the size distributions of the vesicles using dynamic light scattering (DLS). DLS showed that the UC/F procedure yielded a particle distribution with ~20 nm maximum hydrodynamic diameter (Figure 1A). Larger particles, up to ~1000 nm, also were observed, suggesting that the preparation also contained some ectosomes and potentially cell debris. It is important to remember that the contribution of large particles is highly overrepresented by DLS because the intensity of the DLS signal is proportional to the square of the particle mass. The ExoQuick kit yielded a broader size distribution of particles compared to those by UC/F (Figure 1A), comprising three peaks at hydrodynamic diameter ~30, 300, and 6000 nm. These data demonstrated that the ExoQuick preparation contained larger particles, yet suggested that the vast majority of the particles comprising the mixture in both cases were in the 30−200-nm-diameter range, consistent with exosomes.

To further assess the particle size distributions of the two preparations using a method that does not overemphasize larger particles, we used tunable resistive pulse sensing (TRPS). For the UC/F preparation, TRPS showed a single peak with a mean diameter of 135 ± 33 nm and a d90 value of 165 nm (i.e., 90% of the vesicles had a diameter below 165 nm, Figure 1B). The ExoQuick preparation yielded a similar distribution, though as might be expected, the mean diameter was somewhat larger than that of particles obtained by UC/F, 143 ± 47 nm, and the d90 value was 189 (Figure 1C).

We also characterized the morphology of the particles in each preparation by transmission electron microscopy (TEM). TEM showed that exosomes of similar sizes existed in both preparations (Figure 1D, E), yet the ExoQuick-isolated population contained more structures that looked like cell debris. High-resolution images of single exosomes clearly showed the lipid bilayer enclosing them (Figure 1D, E insets). Finally, to confirm that both preparations contained *bona fide* exosomes, we used Western blotting to detect exosomal protein markers Alix, CD9, and CD81 (http://www.exocarta.org) (Figure 1F). Western blotting confirmed that these markers were enriched in both populations compared to the original FBS.

Measurement of the protein content in each preparation using the bicinchoninic acid (BCA) assay showed that the amount of protein in the ExoQuick preparation was ~850 times higher than that in the UC/F preparation. This substantially higher yield represents both the somewhat more heterogeneous nature of the EV population isolated by the ExoQuick kit and the loss of a large portion of the exosomes during the UC/F process.

SERS Hybrid System for Measuring the Raman Spectra of Exosomes. To collect the Raman signature of exosomes, we used a plasmonic substrate consisting of a graphene layer on top of an Au surface with periodic pyramidal structures, heretofore referred to as a "hybrid substrate".[30−32] A schematic of the hybrid substrate is shown in Figure 2A and

DOI: 10.1021/acssensors.8b01564
ACS Sens. XXXX, XXX, XXX−XXX

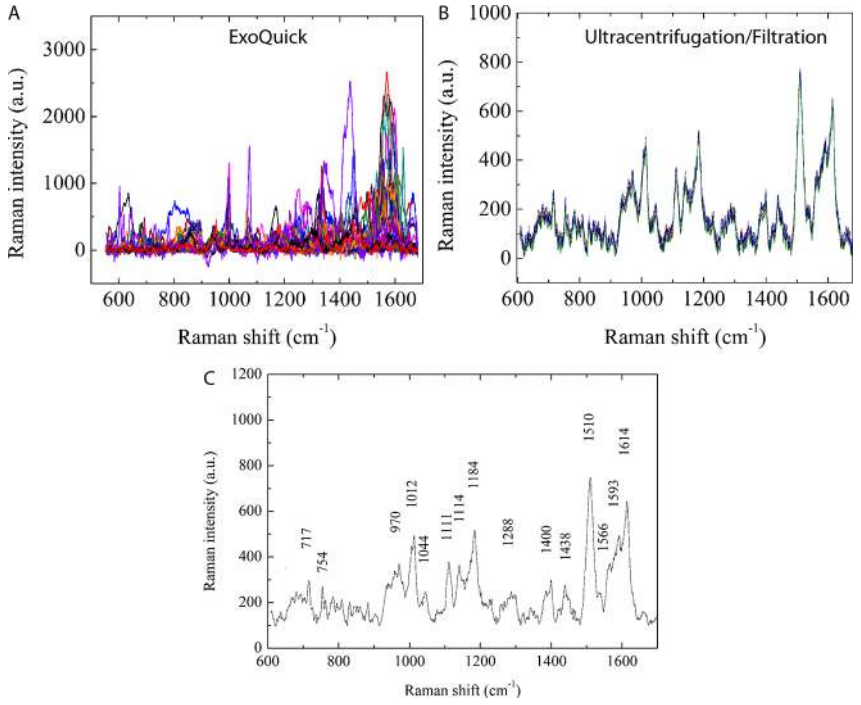

Figure 3. Raman spectra of exosomes collected using the two preparation methods. (A) Raman spectra of exosomes isolated from FBS using the ExoQuick kit. (B) Raman spectra of exosomes isolated from FBS using UC/F. (C) Averaged spectrum of the 100 overlaid spectra in panel B. The wavelengths of assigned peaks are indicated above the peaks themselves.

a top view by scanning electron microscopy (SEM) is provided in Figure 2B. The base dimensions of the pyramids are ~200 × 200 nm^2 and the center-to-center distance between adjacent pyramids is ~400 nm. The angle of the sidewalls of the pyramids is 57.5°, defined by the {111} facets of (001) oriented Si crystal/wafer used to produce the pyramids. Previously, this hybrid substrate was demonstrated to have a Raman enhancement factor of up to 10^{12}.[33]

The quasi-periodic Au nanopyramid structure was fabricated using a patterning method via a layer of self-assembled polystyrene balls, providing a reproducible and uniform SERS response. Such a fabrication process can be easily scaled up for mass production using silicon-integrated-circuit technology.[34] The graphene layer placed on top of the metal surface provides a biocompatible surface, independent of the type of metal used, for supporting plasmon resonance. The local electromagnetic field distribution on the hybrid substrate can be simulated using a finite-difference time-domain method (FDTD).[35] A typical result of such a simulation shows that the hotspots, where the electromagnetic field is highly enhanced, are on each side of the nanopyramids (Figure 2C). The Raman spectrum of the hybrid substrate, reflecting the graphene peaks is shown in Figure 2D.

The graphene layer is chemically inert and impermeable even to He atoms,[36] protecting the metallic nanostructures from possible corrosion, including oxidation, and preventing biological substrates, such as cells, from undesired negative effects of the metal surface. The Raman signal of the graphene layer also serves as a built-in gauge of the local electromagnetic field intensity. By using this built-in gauge, the intensity of Raman peaks in the biological analytes can be correlated uniquely to the amount of the analytes present within a hotspot, as opposed to being a convolution between the local EM field intensity and the amount of the protein. Therefore, the Raman signal intensity from different sets of hybrid substrates or different spots measured on the same substrate can be compared quantitatively by normalizing the signal to the graphene Raman peaks.

After establishing the differences and similarities between the two exosome-preparation methods, we used the hybrid substrate to collect SERS spectra and test if one or both preparation methods yielded useful Raman fingerprint information. The sample volume was adjusted so that the same total protein concentration was used in each case. For each sample, 100 SERS spectra were collected over distinct spots so that no two spectra were collected from the same portion of the sample. The analysis showed a striking difference between the two populations. Although both samples contained the same amount of total protein, the Raman spectra of the ExoQuick preparation (Figure 3A) had a substantially higher absolute intensity than those in the UC/F preparation (Figure 3B), likely due to the contribution of cell debris, protein aggregates, and/or other nonexosome components. In the UC/F preparation, the spectra showed high homogeneity allowing detection of multiple peaks, including minor ones of intensity <50 au. In contrast, overlapping spectra of the ExoQuick preparation yielded a highly heterogeneous picture, in which locating useful representative data was impractical. This analysis made it clear that the ExoQuick preparation could not be used for obtaining SERS fingerprints in this system, whereas the UC/F method offered abundant useful information. To extract the information generated from the SERS analysis of UC/F-isolated exosomes, we averaged the 100 spectra collected (Figure 3B) and could assign 15 distinct peaks in this averaged spectrum (Figure 3C) using known assignments of Raman spectra in biological samples[37] (Table 1).

Though we have chosen to use the ExoQuick kit, other commercial kits exist for isolation of exosomes using similar methods and our data suggest that these kits generally are

DOI: 10.1021/acssensors.8b01564
ACS Sens. XXXX, XXX, XXX−XXX

Table 1. Assignment of the Raman Peaks Shown in the Spectrum in Figure 3

Raman shift (cm^{-1})	Peak assignment	References
716	C−N (membrane phospholipids head)	47, 48
	$CN-(CH_3)_3$ (lipids)	
753	Symmetric breathing of tryptophan	49−51
970	Lipids	52
	Phosphate monoester groups of phosphorylated proteins and nucleic acids	
1012	Phenylalanine	53
1044	Proline	54, 55
	$\nu_3PO_4^{3-}$(symmetric stretching vibration)	
1111	Phenylalanine (proteins)	56
1140	Fatty acids	57
1183	Cytosine, guanine, adenine	30
1287	Cytosine	39
1400	C═O symmetric stretch	58, 59
	CH_2 deformation NH in-plane deformation	
1438	CH_2 and CH_3 deformation vibrations, cholesterol, fatty acid band	60
1510	A (ring-breathing modes in the DNA bases)	29
1566	Tryptophan	61
1592	G (DNA/RNA), CH deformation (proteins, and carbohydrates)	62
1614	C═C stretching mode of tyrosine	30, 38

incompatible with SERS analysis due to inclusion of nonexosome components that decreases the signal-to-noise ratio. It is possible, however, that improved techniques, such as the recent ExoQuick-Ultra kit, which adds another purification step, will yield exosome populations amenable to SERS, and testing such improved methods will be examined in future studies. (In this context, signal-to-noise refers to the reproducible observation of certain Raman peaks from putative single exosomes in the UC/F preparation (Figure 3B) as opposed to the multiple non-overlapping spectra in the ExoQuick preparation, which indicated high sample heterogeneity.)

Considering the results discussed above (Figure 3A, B), we focused the rest of the study on exosomes prepared using the UC/F method. Our next goal was to validate that the Raman spectra measured using the hybrid system were from single exosomes. Because of the small size of the exosomes, 30−200 nm, the limited spatial resolution of an optical microscope attached to the Raman spectrometer did not allow direct visualization of individual exosomes for the purpose of determining the source of the Raman spectra. Therefore, we used SEM, which has sufficient spatial resolution for observing exosomes, but requires a separate measurement. To correlate between SEM visualization and Raman signature measurements, we conducted serial-dilution experiments, in which we used either the unaltered exosome preparation or samples diluted 3- or 10-times. We collected Raman spectra across a 10 × 10-pixel area at each concentration (Figure 4A−C) and visualized the same hybrid substrates by SEM (Figure 4F). The pixel size of the Raman map was set at 2 μm to avoid overlap of adjacent laser spots. The Raman mapping results of the three samples showed a density change consistent with the change of the sample concentration.

As a test for the presence of exosomes in each spectrum, we chose three spectral peaks with high signal-to-noise ratios at 1012 (Figure 4D, red pixels), 1509 (yellow pixels), and 1613

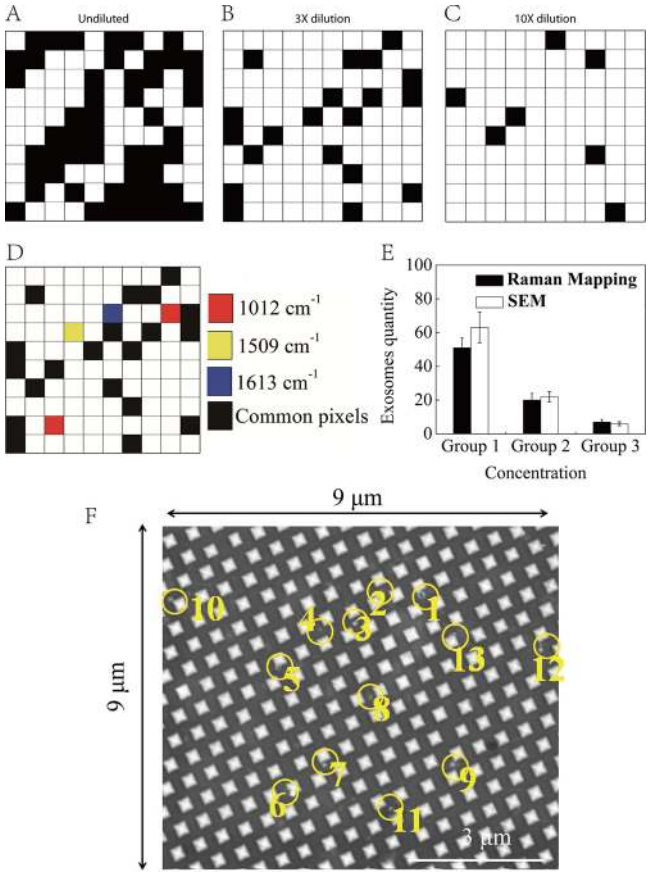

Figure 4. SERS and SEM mapping of exosomes adsorbed on the hybrid substrate. (A−C) Raman mapping of the same undiluted (A), 3-times diluted (B), or 10-times diluted (C) exosome preparation. (D) Pixel assignment for the Raman signature of exosomes. The red, yellow, and blue pixels represent the presence of 1012, 1509, and 1613 cm^{-1} peaks in the Raman spectrum, respectively. The black pixels are those in which all three peaks were detected. Only black pixels were considered as containing exosomes. (E) Comparison of the exosome density obtained through Raman mapping and SEM at three different exosome concentrations. (F) A representative 9 × 9-μm SEM micrograph of exosomes attached to the graphene-covered surface at 35,000× magnification. The yellow circles mark the presence of exosomes within this region.

(blue pixels) cm^{-1} representing the vibrational mode of phenylalanine, the ring-breathing mode in DNA bases, and the Raman mode of tyrosine, respectively. It should be noted that to observe the 1613 cm^{--1} peak, we subtracted the graphene G-peak, which normally masks the 1613 cm^{-1} peak. The position of the graphene G-peak is stably at 1583 cm^{-1} and its intensity can vary depending on the layer number. Here, we used a single-layer graphene with 97% uniformity, measured a background spectrum of the graphene signal in the absence of the biological sample, scaled the intensity so that the amplitude of the G-peak in this background spectrum matched that of the exosome-measurement spectrum, and subtracted the G-peak using the built-in function of Reinshaw WiRe 4.2 software. Such background subtraction is a routine process commonly applied by Raman spectroscopists. As this was a yes/no type of analysis, normalizing to the graphene signal was not necessary in this case.

We postulated that each individual peak in these spectra might represent sources other than exosomes—such as protein aggregates or cell debris—but that appearance of all three

DOI: 10.1021/acssensors.8b01564
ACS Sens. XXXX, XXX, XXX−XXX

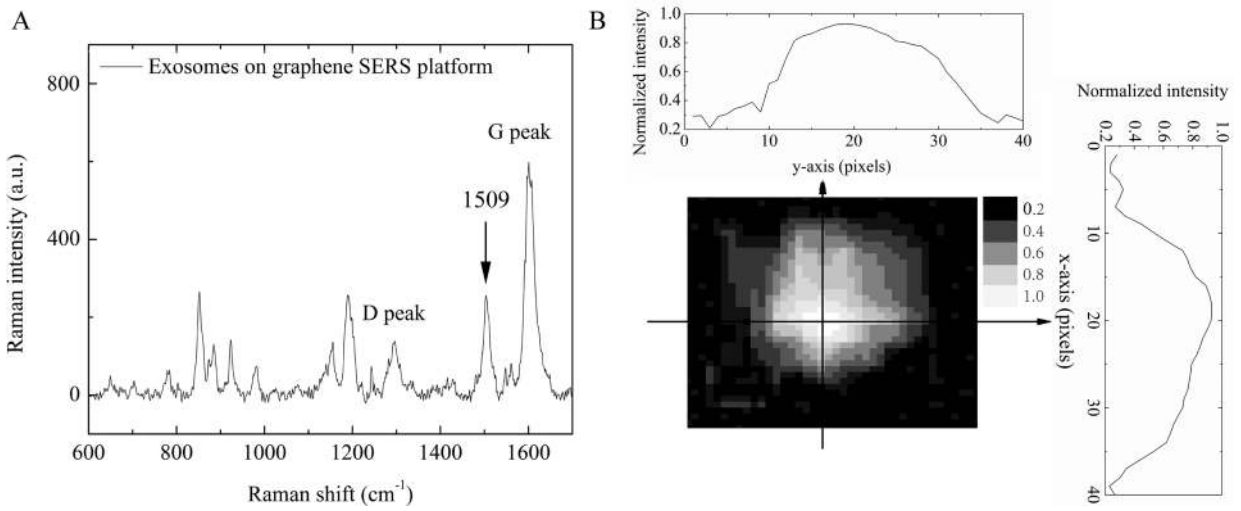

Figure 5. Raman-based topological mapping of an intact individual exosome. (A) Raman spectrum used for generating the topological map. The graphene D and G peaks and the DNA-base ring-breathing peak at 1509 cm^{-1} used for generating the map are indicated. (B) Topological map based on the 1509 cm^{-1} peak using a step size of 0.1 μm. The peak-intensity changes along the *x*- and *y*-axes are shown on the right and top, respectively.

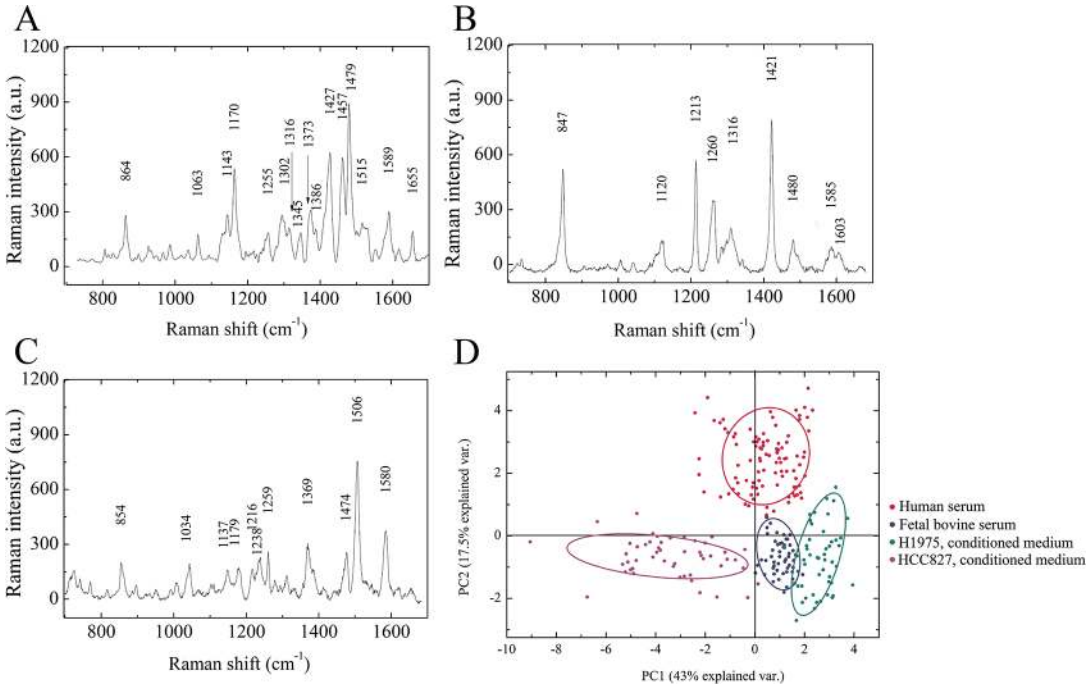

Figure 6. SERS analysis and PCA of exosomes from different sources. (A–C) Raman spectra of exosomes from human serum (A) conditioned medium of the lung-cancer cell line HCC827 (B), and conditioned medium of the lung-cancer cell line H1975 (C). (D) PCA of exosomes from the different sources shown in panels A–C and the spectrum shown in Figure 3C demonstrating that they are distinguishable.

peaks in the same spectrum likely represented *bona fide* exosomes. Figure 4D demonstrates that the majority of the pixels yielding a Raman spectrum other than that of only graphene contained all three peaks (represented as black pixels), suggesting that the source of the spectrum in each of these pixels was an exosome. As expected, the Raman mapping demonstrated that the density of the black pixels decreased proportionally with increasing dilution.

After measuring the Raman signature, we used SEM to determine visually the location of the exosomes on the hybrid substrate at the same dilutions, counted the exosome number within randomly selected, 9 × 9 μm^2 areas (Figure 4F), and compared the exosome density with the Raman mapping results. The exosome density at each concentration was determined by averaging measurements at ten different areas. Comparison of the exosome density obtained separately using Raman mapping and SEM showed a strong correlation between the two methods (Figure 4E). The two measurements showed similar exosome density at each dilution and the difference between them was statistically insignificant (p = 0.385, two-way ANOVA). In contrast, the difference among the three dilutions measured by each method was statistically significant (p = 0.017).

DOI: 10.1021/acssensors.8b01564
ACS Sens. XXXX, XXX, XXX–XXX

Estimation of Exosome Morphology Using High-Resolution Raman Mapping. In the Raman mapping shown in Figure 4, we observed variation in the intensity of the Raman signal from pixel to pixel, primarily due to the existence of exosomes in some pixels but not others. In addition, the magnitude of the signal depends on the Gaussian-shaped exciting laser beam and the proximity of the sample to the hotspots on the sides of the Au pyramids where the SERS enhancement is maximal (Figure 1C). Although the data discussed above supported the interpretation that the Raman spectra were collected from *bona fide* exosomes, they could not rule out the possibility that the spectra reflected a small cell fragment that happens to contain both proteins and DNA. To test further if the data were obtained from exosomes, we reasoned that unlike the spherical shape of exosomes, the likelihood that cell fragments would be spherical was low. Therefore, we mapped the topology of the structures giving rise to the Raman spectra using the intensity of the Raman spectrum itself by performing high-spatial-resolution Raman mapping with 0.1-μm fine-step size (Figure 5). Examination of the Raman spectra emanating from a single source on the surface of the hybrid substrate showed multiple peaks, among which the graphene G-peak was easily identified (Figure 5A). In this set of experiments, we did not subtract this peak, but rather used it to normalize the Raman signal intensity at each laser-beam step to eliminate the influence of unavoidable hotspot intensity fluctuations. Therefore, the peak at 1613 cm^{-1} used in the previous experiments (Figure 4) was not included in this morphological analysis. Because the 1509 cm^{-1} peak was the more intense of the two remaining peaks (Figure 5A), we used the intensity of this peak to generate a topological map based on the intensity of the signal at each step and reconstructed a 3-D map of peak-intensity changes along the *x*- and *y*-axes (Figure 5B). The resulting high-resolution topological map showed a quasi-spherical structure supporting the notion that the Raman spectra indeed were collected from individual exosomes. Because the diameter of the exosomes, 30−200 nm, is smaller than that of the laser beam, ∼1 μm, the measurement did not allow precise measurement of exosome diameter.

SERS Platform Distinguishes Exosomes from Different Sources. Spectral features of SERS are highly sensitive to the chemical composition of biomolecules. After establishing that the SERS spectra likely represented single exosomes, we asked whether this sensitivity could translate to specificity, distinguishing exosomes from different sources. This question is critical for determining the potential value of the SERS platform for biomedical applications. To address this question, we compared the spectra of exosomes from different sources: First, we asked if the FBS used for the initial characterization up to this point (Figure 3C) could be distinguished from human serum (Figure 6A); second, we asked whether the human serum exosome spectra could separate them from those in the conditioned tissue-culture medium of a human lung cancer cell line; and finally, as a highly difficult challenge for the platform, whether the specificity could be extended to distinguishing between two lung cancer cell lines, HCC827 (Figure 6B) and H1975 (Figure 6C). We collected 100 Raman spectra from each sample and assigned all of the identified peaks—corresponding expectedly to nucleic acids, proteins, and lipids—and showing both similarities and differences. The complete peak assignments are provided in Supplementary Tables S1 (human serum), S2 (HCC827), and S3 (H1975).

Each sample showed uniquely identifiable spectral characteristics distinguished primarily by the relative peak intensities. For example, the relative intensity of nucleic-acid bands was substantially higher in the human-serum- and FBS-derived exosomes compared to those from the conditioned media of the cancer cell lines. The reason for this difference is not known at this time and will be explored in future studies. In contrast, the relative intensity of the lipid bands was clearly higher in exosomes derived from cancer cells, in agreement with previous reports suggesting that cancer cells store excessive amounts of lipids and cholesterol in lipid droplets, making this feature a hallmark of aggressive cancers.[38−40] We then used PCA to analyze spectral differences and similarities in ∼50 Raman spectra from each sample (Figure 6D). The results showed that the exosomes from all four different sources clustered into distinguishable groups with <5% overlap among the groups at a sensitivity of >84%. Interestingly, the largest degree of overlap was not between the two sera or the two cell lines, but between FBS and the H1975 cell line (Figure 6D). These findings suggest that analysis of exosomes from the serum of two different species, cell culture media versus serum, and cell culture media from two cancer cell lines of the same human organ, lung, can be distinguished using our platform. The data suggest that the methodology and platform developed here have the potential of serving as a unique biomarker, without requiring knowledge of disease mechanism, defining specific candidate biomarkers, or using biological labels. It should be further pointed out that the ability to distinguish subtle differences among Raman spectra from different sources is highly dependent on the data analysis algorithm. For our study, a more advanced algorithm such as deep neural network may allow in the future to achieve better separation than that achievable using PCA.

Recently, a few groups have applied SERS to characterize exosomes,[41−44] yet to our knowledge, our study is the first to demonstrate acquisition of Raman spectra from single exosomes and differentiating the exosomes from other EVs and fragments of various biological entities.

CONCLUSION

We have demonstrated the potential of a new SERS-based platform for identification of exosomes from readily available biological samples and obtaining unique fingerprint signatures from these exosomes. We showed the reproducibility of the spectra when the exosomes are isolated by the UC/F method (Figure 3B) and the fingerprinting capability of the platform by comparing the spectra of exosomes from four different sources. Using PCA, the platform clusters the spectra of exosomes into readily distinguishable groups with <5% overlap among different groups at a sensitivity of >84%, which to our knowledge is higher than what has been reported to date. As an inherently single-exosome-based and label-free methodology, the platform holds tremendous and realistic promise for identifying specific biomarkers for early stage diagnosis and a useful research tool for deepening the understanding of the role of exosomes in normal physiology and disease.

EXPERIMENTAL METHODS

Fabrication of Au Nanopyramid Hybrid SERS Substrate. The hybrid SERS substrate used here was prepared as described previously.[31] Briefly, we generated a template using a single layer of self-assembled polystyrene balls. The near-hexagonal pitch periodicity was then transferred to a SiO_2 mask over a Si (001) wafer via plasma

DOI: 10.1021/acssensors.8b01564
ACS Sens. XXXX, XXX, XXX−XXX

etching. These two methods produce nanometer-scale, 2-D features of poorly defined shapes. We employed an additional step of anisotropic etching of Si to transfer the fuzzy 2-D features into well-defined 3-D-inverted pyramids with facets consisting of {111} planes on a (001) oriented Si wafer.[45] The angle of the sidewalls of the pyramids relative to their basal plane is 57.5°, determined using crystallography of the Si crystal. We further employed geometrical hindrance during thermal oxidation of Si to fine-tune the sharpness of the apex of the inverted pyramids.[39] 200-nm-thick Au films then were deposited over the pitted surface, bonded to a handle substrate using epoxy, and then lifted off the surface thereby completing the nanocasting process. Because of the way the substrate was fabricated, the Au-tipped surface had the unique features of in-plane anisotropy and wafer-scale coherence with the precise orientation and shape of individual pyramids.

Preparation and Transfer of Graphene. 25-μm-thick copper foil was cut into a 2 × 2-in. square and placed at the center of a quartz chemical vapor deposition (CVD) tube of 15 cm diameter to serve as a catalyst during CVD growth. The furnace was heated to ∼1060 °C under H_2 flow at 1 Torr total pressure. After 30 min annealing, growth commenced under 20 Torr total pressure with a flow of CH_4 (∼20 standard cubic centimeter per minute (sccm)) and H_2 (∼1000 sccm) for 15 min. The chamber was cooled down to room temperature over 10 h. A ∼500 nm poly(methyl methacrylate) (PMMA) layer was spin-coated on the graphene-covered Cu foil to provide mechanical support to the graphene monolayer during the subsequent Cu-etching step. The Cu foil was removed in an etching solution of $FeCl_3$:H_2O (1:5 vol %). Then, the floating PMMA−graphene structure was transferred onto the surface of deionized water and the sample was transferred onto a target substrate. In the final step, the PMMA-supporting layer was removed by acetone.

Raman Spectroscopy. Raman spectra were recorded using a Renishaw inVia Raman spectrometer under ambient conditions (20 °C and 1 atm). WiRe 4.2 software was used to control the entire system. The laser excitation wavelength was 785 nm, which generates a low fluorescence background but still has a strong localized electromagnetic field.[24] The power of the laser was kept at 5 mW to avoid sample overheating. The diameter of the laser spot was 1.8 μm. The Raman measurements were calibrated first by the Si Raman mode at 520 cm^{-1}. Then, 2 μL of the exosome solutions were applied to the hybrid platform surface and allowed to air-dry before the measurement. The acquisition time was 1 s. For coarse Raman mapping, Raman spectra across a 10 × 10-pixel area were collected with a step length of 2 μm. For fine Raman mapping, Raman spectra across a 10 × 10-pixel area were collected with a step length of 0.1 μm. The acquisition time was 0.2 s to avoid overheating.

Exosome Isolation. FBS was purchased from Invitrogen, USA. For human serum, peripheral blood was collected from a healthy volunteer by venipuncture using a BD Vacutainer push-button blood collection kit and left to coagulate in silicone-coated serum collection tubes for 20 min at room temperature. After centrifugation at 1500 × g for 15 min, the serum was collected and either processed immediately or stored at −80 °C. The human lung cancer cell lines, HCC827 and H1975, were obtained from ATCC and cultured in 75 cm^2 tissue-culture flasks. Cells were cultured in exosome-free conditioned medium, pre-cleared of exosomes and protein aggregates before use for cell culture by ultracentrifugation. Supernates were collected 48−72 h after changing the medium for exosome isolation.[46] EVs from FBS were isolated using an ExoQuick kit (System Biosciences, USA) following the manufacturer's instructions.

For isolation of exosomes using the UC/F method, after thawing quickly in a 37 °C water bath, protease and phosphatase inhibitors were added and the serum/media from either source was diluted five times in chilled PBS. Cell culture supernates or diluted sera were centrifuged at 2000 × g and 4 °C for 20 min and then further centrifuged at 12,000 × g and 4 °C for 45 min to remove small debris. The supernates were filtered using 0.22-μm-pore filters, followed by ultracentrifugation in a Model L8-M70 ultracentrifuge (Beckman Coulter, USA) at 110,000 × g and 4 °C for 2 h. The resulting pellets were resuspended in chilled PBS and ultracentrifuged again at 110,000 × g and 4 °C for 70 min. The final pellet of exosomes was resuspended in 50−100 μL chilled PBS for TRPS measurement, in a 2% glutaraldehyde or 2% paraformaldehyde (PFA) solution in Milli-Q water for SERS and TEM experiments, respectively, or lysed in RIPA buffer, aliquoted, and stored at −80 °C for Western blot analysis.

Dynamic Light Scattering. The size distribution (hydrodynamic diameter) of exosomes was determined using a Zetasizer Nano instrument (Malvern Instruments Ltd., Worcestershire, UK). After isolation, the exosome pellet was reconstituted in 100 μL of filtered PBS. 50 μL of purified exosomes were diluted in 1450 μL of filtered PBS and gently vortexed for 30 s to avoid aggregation. The whole volume was quickly transferred into a disposable cuvette and allowed to equilibrate for 30 s at 25 °C. A 20 mW He−Ne laser operating at 632 nm was used at an angle of 173°. The dispersant refractive index value used was 1.37. The size of the observed particle populations was determined by Z-average and polydispersity index (PdI). Three independent measurements of 14 counts each were performed per sample and average values are presented.

Tunable Resistive Pulse Sensing (TRPS). TRPS measurements were performed using a qNano instrument (Izon Science, Christchurch, New Zealand) equipped with a polyurethane nanopore axially stretched to 48 mm (NP150, Izon Science, UK). All measurements were calibrated with appropriately diluted CPC200 polystyrene beads (Izon Science, UK). 40 μL samples diluted in PBS were used for measurement. Data were processed and analyzed using the Izon Control Suite software v 3.3.2.2001.

Transmission Electron Microscopy (TEM). For TEM examination of isolated exosomes, pellets obtained after the last centrifugation step were resuspended in fixative (2% PFA in Milli-Q water). Formvar carbon-coated grids (FCF400-CU, Electron Microscopy Sciences) were glow-discharged on a Pelco easiGlow instrument (Ted Pella Inc., USA) for 2 min. Small drops of PFA-fixed exosomes then were placed on the grids and incubated for 20 min. The grids were washed by floating them upside down on drops of deionized water. The exosomes were further fixed in 1% glutaraldehyde for 5 min and then stained successively in freshly prepared 2% uranyl acetate and 2% methylcellulose/0.4% uranyl acetate. Grids were imaged using a FEI Technai T20 transmission electron microscope equipped with a thermionic tungsten filament and operated at an acceleration voltage of 200 kV. Images were taken using a cooled slow-scan CCD camera at a magnification of 80,000× or 100,000×.

Scanning Electron Microscopy (SEM). SEM imaging was performed using a Nova 230 Nano scanning electron microscope. The accelerating voltage was 10 kV. The samples were viewed at an electron spot size of three. The detector mode was "through-the-lens" secondary electron detector. The SERS substrate was mounted on the stage by double-coated carbon-conductive tape. Images were taken at a magnification of 35,000× or 50,000×.

Western Blotting. Protein concentration was estimated using a BCA protein-assay kit (ThermoFisher Scientific, USA). Proteins were mixed with NuPAGE LDS Sample Buffer containing 5% β-mercaptoethanol and heated at 90 °C for 10 min. 20 μg of protein extracts were fractionated on 4−12% NuPAGE Bis-Tris gels and electrotransferred onto nitrocellulose membranes (ThermoFisher Scientific, USA). The membranes were then blocked in 5% skim milk in tris-buffered saline containing 0.1% Tween-20 (TBST) for 1 h at room temperature and then were incubated overnight at 4 °C with appropriate primary antibodies at 1:2000 dilution in blocking solution. After three washes with TBST for 10 min each, horseradish-peroxidase-conjugated secondary antibodies (Thermo-Fisher Scientific) at 1:5000 dilution in blocking solution were added, and the membranes were incubated for 1 h at room temperature. SuperSignal West Femto maximum sensitivity substrate (Thermo Fisher Scientific, USA) was added, and protein bands were visualized using a Gel-Doc apparatus (Syngene, USA).

Statistical and Principal Component Analyses. Statistical analysis was done using Origin 8.0. Results were considered significant at $p < 0.05$. PCA is a statistical procedure that uses an orthogonal transformation to convert a set of observations of possibly correlated variables into a set of values of linearly uncorrelated

DOI: 10.1021/acssensors.8b01564
ACS Sens. XXXX, XXX, XXX−XXX

variables called principal components (or sometimes, principal modes of variation). In our study, the correlated variables were the vectors including Raman shift and the related Raman intensity of each Raman spectrum. This orthogonal transformation was defined so that the first principal component (PC1) had the largest possible variance (i.e., accounted for as much of the variability in the data as possible), and each succeeding component (PC2, PC3, etc.) in turn had the highest variance possible under the constraint that it is orthogonal to the preceding components. The results are presented using PC1 and PC2 (Figure 6D). To obtain these results, first, the background of the Raman spectrum was subtracted and the data were saved in .txt format. Then, PCA analysis was performed using an in-house-coded program running on a Python compiler. Sixteen vectors were chosen along the Raman shift axis (847, 854, 1043, 1163, 1181, 1202, 1213, 1255, 1269, 1309, 1374, 1384, 1421, 1429, 1482, and 1506 cm^{-1}) for fully regenerating the original spectra. The data were visualized using an in-house-written program in R Studio.

■ ASSOCIATED CONTENT

Supporting Information

The Supporting Information is available free of charge on the ACS Publications website at DOI: 10.1021/acssensors.8b01564.

Three tables of Raman peak assignments and corresponding references (PDF)

■ AUTHOR INFORMATION

Corresponding Authors

*E-mail: gbitan@mednet.ucla.edu. Phone: 310-206-2082.
*E-mail: yhx@ucla.edu. Phone: (310)259-6946.

ORCID

Gal Bitan: 0000-0001-7046-3754

Author Contributions

#Z. Y. and S. D. contributed equally to the work.

Notes

The authors declare no competing financial interest.

■ ACKNOWLEDGMENTS

We thank Dr. Farid Rahimi, Australian National University, Canberra, for editorial help. This work was funded by a grant from the United States Government and the generous support of the American people through the United States Department of State and the United States Agency for International Development (USAID) under the Pakistan−U.S Science & Technology Cooperation Program. The contents do not necessarily reflect the views of the United States Government. Y.H.X. acknowledges partial support from Zhejiang University Cao Guang-Biao Advanced Science and Technology Fund and from an Alexander von Humboldt Foundation Research Award. G.B. acknowledges support from Team Parkinson/Parkinson Alliance, a pilot grant from the UCLA American Parkinson's Disease Association (APDA) Center, and grant 2017-10-007 from the MSA Coalition.

■ REFERENCES

(1) Théry, C.; Ostrowski, M.; Segura, E. Membrane vesicles as conveyors of immune responses. *Nat. Rev. Immunol.* **2009**, *9* (8), 581−593.

(2) van der Pol, E.; Böing, A. N.; Harrison, P.; Sturk, A.; Nieuwland, R. Classification, functions, and clinical relevance of extracellular vesicles. *Pharmacol. Rev.* **2012**, *64* (3), 676−705.

(3) Pilzer, D.; Gasser, O.; Moskovich, O.; Schifferli, J. A.; Fishelson, Z. Emission of membrane vesicles: roles in complement resistance, immunity and cancer. *Springer Semin. Immunopathol.* **2005**, *27* (3), 375−387.

(4) Johnstone, R. M. Exosomes biological significance: a concise review. *Blood Cells, Mol., Dis.* **2006**, *36* (2), 315−321.

(5) Taylor, D. D.; Gercel-Taylor, C. MicroRNA signatures of tumor-derived exosomes as diagnostic biomarkers of ovarian cancer. *Gynecol. Oncol.* **2008**, *110* (1), 13−21.

(6) Vlassov, A. V.; Magdaleno, S.; Setterquist, R.; Conrad, R. Exosomes: current knowledge of their composition, biological functions, and diagnostic and therapeutic potentials. *Biochim. Biophys. Acta, Gen. Subj.* **2012**, *1820* (7), 940−948.

(7) Simpson, R. J.; Lim, J. W.; Moritz, R. L.; Mathivanan, S. Exosomes: proteomic insights and diagnostic potential. *Expert Rev. Proteomics* **2009**, *6* (3), 267−283.

(8) Rabinowits, G.; Gerçel-Taylor, C.; Day, J. M.; Taylor, D. D.; Kloecker, G. H. Exosomal microRNA: a diagnostic marker for lung cancer. *Clin. Lung Cancer* **2009**, *10* (1), 42−46.

(9) Michael, A.; Bajracharya, S. D.; Yuen, P. S.; Zhou, H.; Star, R. A.; Illei, G. G.; Alevizos, I. Exosomes from human saliva as a source of microRNA biomarkers. *Oral Dis.* **2010**, *16* (1), 34−38.

(10) Théry, C.; Amigorena, S.; Raposo, G.; Clayton, A. Isolation and characterization of exosomes from cell culture supernatants and biological fluids. *Curr. Protoc. Cell Biol.* **2006**, *30*, 3−22.

(11) Théry, C.; Regnault, A.; Garin, J.; Wolfers, J.; Zitvogel, L.; Ricciardi-Castagnoli, P.; Raposo, G.; Amigorena, S. Molecular characterization of dendritic cell-derived exosomes. *J. Cell Biol.* **1999**, *147* (3), 599−610.

(12) Lamparski, H. G.; Metha-Damani, A.; Yao, J. Y.; Patel, S.; Hsu, D. H.; Ruegg, C.; Le Pecq, J. B. Production and characterization of clinical grade exosomes derived from dendritic cells. *J. Immunol. Methods* **2002**, *270* (2), 211−226.

(13) Conde-Vancells, J.; Rodriguez-Suarez, E.; Embade, N.; Gil, D.; Matthiesen, R.; Valle, M.; Elortza, F.; Lu, S. C.; Mato, J. M.; Falcon-Perez, J. M. Characterization and comprehensive proteome profiling of exosomes secreted by hepatocytes. *J. Proteome Res.* **2008**, *7* (12), 5157−5166.

(14) Notingher, I. Raman spectroscopy cell-based biosensors. *Sensors* **2007**, *7* (8), 1343−1358.

(15) Lawson, E. E.; Barry, B. W.; Williams, A. C.; Edwards, H. G. M. Biomedical applications of Raman spectroscopy. *J. Raman Spectrosc.* **1997**, *28* (2−3), 111−117.

(16) Kneipp, K.; Kneipp, H.; Itzkan, I.; Dasari, R. R.; Feld, M. S. Ultrasensitive chemical analysis by Raman spectroscopy. *Chem. Rev.* **1999**, *99* (10), 2957−2976.

(17) Stiles, P. L.; Dieringer, J. A.; Shah, N. C.; Van Duyne, R. P. Surface-enhanced Raman spectroscopy. *Annu. Rev. Anal. Chem.* **2008**, *1*, 601−626.

(18) Garrell, R. L. Surface-enhanced Raman spectroscopy. *Anal. Chem.* **1989**, *61* (6), 401A−411A.

(19) Yan, Z.; Xia, M.; Zhang, P.; Xie, Y. H. Self-aligned trapping and detecting molecules using a plasmonic tweezer with an integrated electrostatic cell. *Adv. Opt. Mater.* **2017**, *5* (5), 1600329.

(20) Moskovits, M. Surface-enhanced Raman spectroscopy: a brief retrospective. *J. Raman Spectrosc.* **2005**, *36* (6−7), 485−496.

(21) Moskovits, M. Surface-enhanced spectroscopy. *Rev. Mod. Phys.* **1985**, *57* (3), 783−826.

(22) Wang, P.; Xia, M.; Liang, O.; Sun, K.; Cipriano, A. F.; Schroeder, T.; Liu, H.; Xie, Y. H. Label-free SERS selective detection of dopamine and serotonin using graphene-Au nanopyramid heterostructure. *Anal. Chem.* **2015**, *87* (20), 10255−10261.

(23) Liang, O.; Wang, P.; Xia, M.; Augello, C.; Yang, F.; Niu, G.; Liu, H.; Xie, Y. H. Label-free distinction between p53+/+ and p53−/−colon cancer cells using a graphene based SERS platform. *Biosens. Bioelectron.* **2018**, *118*, 108−114.

(24) Pinto, A. M.; Goncalves, I. C.; Magalhães, F. D. Graphene-based materials biocompatibility: a review. *Colloids Surf., B* **2013**, *111*, 188−202.

DOI: 10.1021/acssensors.8b01564
ACS Sens. XXXX, XXX, XXX−XXX

(25) Chen, H.; Müller, M. B.; Gilmore, K. J.; Wallace, G. G.; Li, D. Mechanically strong, electrically conductive, and biocompatible graphene paper. *Adv. Mater.* **2008**, *20* (18), 3557−3561.
(26) Yi, N.; Zhang, C.; Song, Q.; Xiao, S. A hybrid system with highly enhanced graphene SERS for rapid and tag-free tumor cells detection. *Sci. Rep.* **2016**, *6*, 25134.
(27) Ren, W.; Fang, Y.; Wang, E. A binary functional substrate for enrichment and ultrasensitive SERS spectroscopic detection of folic acid using graphene oxide/Ag nanoparticle hybrids. *ACS Nano* **2011**, *5* (8), 6425−6433.
(28) System Bioscience, LLC. https://www.systembio.com/products/exosome-research/exosome-isolation/exoquick-tc/.
(29) Helwa, I.; Cai, J.; Drewry, M. D.; Zimmerman, A.; Dinkins, M. B.; Khaled, M. L.; Seremwe, M.; Dismuke, W. M.; Bieberich, E.; Stamer, W. D.; Hamrick, M. W.; Liu, Y. Comparative study of serum exosome isolation using differential ultracentrifugation and three commercial reagents. *PLoS One* **2017**, *12* (1), e0170628.
(30) Wang, P.; Zhang, W.; Liang, O.; Pantoja, M.; Katzer, J.; Schroeder, T.; Xie, Y. H. Giant optical response from graphene−plasmonic system. *ACS Nano* **2012**, *6* (7), 6244−6249.
(31) Xia, M.; Zhang, P.; Qiao, K.; Bai, Y.; Xie, Y. H. Coupling SPP with LSPR for enhanced field confinement: A simulation study. *J. Phys. Chem. C* **2016**, *120* (1), 527−533.
(32) Xia, M.; Qiao, K.; Cheng, Z.; Xie, Y. H. Multiple layered metallic nanostructures for strong surface-enhanced Raman spectroscopy enhancement. *Appl. Phys. Express* **2016**, *9* (6), 065001.
(33) Wang, P.; Liang, O.; Zhang, W.; Schroeder, T.; Xie, Y. H. Ultrasensitive graphene-plasmonic hybrid platform for label-free detection. *Adv. Mater.* **2013**, *25* (35), 4918−4924.
(34) Heck, M. J.; Bauters, J. F.; Davenport, M. L.; Doylend, J. K.; Jain, S.; Kurczveil, G.; Srinivasan, S.; Tang, Y.; Bowers, J. E. Hybrid silicon photonic integrated circuit technology. *IEEE J. Sel. Top. Quantum Electron.* **2013**, *19* (4), 6100117−6100117.
(35) Lumerical Solutions, Inc. http://www.lumerical.com/tcad-products/fdtd/.
(36) Tamtögl, A.; Bahn, E.; Zhu, J.; Fouquet, P.; Ellis, J.; Allison, W. Graphene on Ni (111): electronic corrugation and dynamics from helium atom scattering. *J. Phys. Chem. C* **2015**, *119* (46), 25983−25990.
(37) Movasaghi, Z.; Rehman, S.; Rehman, I. U. Raman spectroscopy of biological tissues. *Appl. Spectrosc. Rev.* **2007**, *42* (5), 493−541.
(38) Qiu, B.; Ackerman, D.; Sanchez, D. J.; Li, B.; Ochocki, J. D.; Grazioli, A.; Bobrovnikova-Marjon, E.; Diehl, J. A.; Keith, B.; Simon, M. C. HIF2α-dependent lipid storage promotes endoplasmic reticulum homeostasis in clear-cell renal cell carcinoma. *Cancer Discovery* **2015**, *5* (6), 652−667.
(39) Yue, S.; Li, J.; Lee, S. Y.; Lee, H. J.; Shao, T.; Song, B.; Cheng, L.; Masterson, T. A.; Liu, X.; Ratliff, T. L.; Cheng, J. X. Cholesteryl ester accumulation induced by PTEN loss and PI3K/AKT activation underlies human prostate cancer aggressiveness. *Cell Metab.* **2014**, *19* (3), 393−406.
(40) Bozza, P. T.; Viola, J. P. Lipid droplets in inflammation and cancer. *Prostaglandins, Leukotrienes Essent. Fatty Acids* **2010**, *82* (4), 243−250.
(41) Smith, Z. J.; Lee, C.; Rojalin, T.; Carney, R. P.; Hazari, S.; Knudson, A.; Lam, K.; Saari, H.; Ibañez, E. L.; Viitala, T.; Laaksonen, T.; Yliperttula, M.; Wachsmann-Hogiu, S. Single exosome study reveals subpopulations distributed among cell lines with variability related to membrane content. *J. Extracell. Vesicles* **2015**, *4* (1), 28533.
(42) Krafft, C.; Wilhelm, K.; Eremin, A.; Nestel, S.; von Bubnoff, N.; Schultze-Seemann, W.; Popp, J.; Nazarenko, I. A specific spectral signature of serum and plasma-derived extracellular vesicles for cancer screening. *Nanomedicine* **2017**, *13* (3), 835−841.
(43) Kerr, L. T.; Gubbins, L.; Gorzel, K. W.; Sharma, S.; Kell, M.; McCann, A.; Hennelly, B. M. Raman spectroscopy and SERS analysis of ovarian tumor derived exosomes (TEXs): a preliminary study. *Proc. SPIE* **2014**, 91292Q International Society for Optics and Photonics. .
(44) Stremersch, S.; Marro, M.; Pinchasik, B. E.; Baatsen, P.; Hendrix, A.; De Smedt, S. C.; Loza-Alvarez, P.; Skirtach, A. G.; Raemdonck, K.; Braeckmans, K. Identification of individual exosome-like vesicles by surface enhanced Raman spectroscopy. *Small* **2016**, *12* (24), 3292−3301.
(45) Xia, M.; Zhang, P.; Leung, C.; Xie, Y. H. SERS optical fiber probe with plasmonic end-facet. *J. Raman Spectrosc.* **2017**, *48* (2), 211−216.
(46) Dutta, S.; Reamtong, O.; Panvongsa, W.; Kitdumrongthum, S.; Janpipatkul, K.; Sangvanich, P.; Piyachaturawat, P.; Chairoungdua, A. Proteomics profiling of cholangiocarcinoma exosomes: A potential role of oncogenic protein transferring in cancer progression. *Biochim. Biophys. Acta, Mol. Basis Dis.* **2015**, *1852*, 1989−1999.
(47) Notingher, I.; Green, C.; Dyer, C. Discrimination between ricin and Sulphur mustard toxicity in vitro using Raman spectroscopy. *J. R. Soc., Interface* **2004**, *1*, 79−90.
(48) Stone, N.; Kendall, C.; Smith, J.; Crow, P.; Barr, H. Raman spectroscopy for identification of epithelial cancers. *Faraday Discuss.* **2004**, *126*, 141−157.
(49) Huang, Z.; McWilliams, A.; Lui, M.; McLean, D. I.; Lam, S.; Zeng, H. Near-infrared Raman spectroscopy for optical diagnosis of lung cancer. *Int. J. Cancer* **2003**, *107*, 1047−1052.
(50) Stone, N.; Kendall, C.; Shepherd, N.; Crow, P.; Barr, H. Near-infrared Raman spectroscopy for the classification of epithelial pre-cancers and cancers. *J. Raman Spectrosc.* **2002**, *33*, 564−573.
(51) Cheng, W.-T.; Liu, M.-T.; Liu, H.-N.; Lin, S. Y. Micro-Raman spectroscopy used to identify and grade human skin pilomatrixoma. *Microsc. Res. Tech.* **2005**, *68*, 75−79.
(52) Dukor, R. K. Vibrational spectroscopy in the detection of cancer. *Biomedical Applications* **2002**, *5*, 3335−3359.
(53) Naumann, D. Infrared and NIR Raman spectroscopy in medical microbiology. *Proc. SPIE* **1998**, *3257*, 245−257.
(54) Frank, C. J.; McCreery, R. L.; Redd, D. C. B. Raman spectroscopy of normal and diseased human breast tissues. *Anal. Chem.* **1995**, *67*, 777−783.
(55) Cheng, W.-T.; Liu, M.-T.; Liu, H.-N.; Lin, S. Y. Micro-Raman spectroscopy used to identify and grade human skin pilomatrixoma. *Microsc. Res. Tech.* **2005**, *68*, 75−79.
(56) Lakshimi, R. J.; Kartha, V. B.; Krishna, C. M.; Solomon, J. G. R.; Ullas, G.; Uma Devi, P. Tissue Raman spectroscopy for the study of radiation damage: Brain irradiation of mice. *Radiat. Res.* **2002**, *157*, 175−182.
(57) Krafft, C.; Neudert, L.; Simat, T.; Salzer, R. Near infrared Raman spectra of human brain lipids. *Spectrochim. Acta, Part A* **2005**, *61*, 1529−1535.
(58) Faolain, E. O.; Hunter, M. B.; Byrne, J. M.; Kelehan, P.; McNamer, M.; Byrne, H. J.; Lyng, F. M. A study examining the effects of tissue processing on human tissue sections using vibrational spectroscopy. *Vib. Spectrosc.* **2005**, *38*, 121−127.
(59) Farguharson, S.; Shende, C.; Inscore, F. E.; Maksymiuk, P.; Gift, A. Analysis of 5-fluorouracil in saliva using surface-enhanced Raman spectroscopy. *J. Raman Spectrosc.* **2005**, *36*, 208−212.
(60) Hanlon, E. B.; Manoharan, R.; Koo, T.-W.; Shafer, K. E.; Motz, J. T.; Fitzmaurice, M.; Kramer, J. R.; Itzkan, I.; Dasari, R. R.; Feld, M. S. Prospects for in vivo Raman spectroscopy. *Phys. Med. Biol.* **2000**, *45*, 1−59.
(61) Lau, D. P.; Huang, Z.; Lui, H.; Man, C. S.; Berean, K.; Morrison, M. D.; Zeng, H. Raman spectroscopy for optical diagnosis in normal and cancerous tissue of the nasopharynx—Preliminary findings. *Lasers Surg. Med.* **2003**, *32*, 210−214.
(62) Naumann, D. Infrared and NIR Raman spectroscopy in medical microbiology. *Proc. SPIE* **1998**, *3257*, 245−257.

DOI: 10.1021/acssensors.8b01564
ACS Sens. XXXX, XXX, XXX−XXX